Liquid mixing intensification by adding swirling flow in the transverse jet mixer

Bin Wu[†], Chunhui Li[†], Mengxue Zhang and Peicheng Luo[*]

School of Chemistry & Chemical Engineering, Southeast University, 211189 Nanjing, China

Submitted to AIChE Journal

November 2020

[†] Wu B. and Li C. contributed equally to this work.

* Corresponding author. Email: luopeicheng@seu.edu.cn

Abstract

In this study, effect of swirling addition on the liquid mixing behavior of multi-orifice-impinging transverse jet mixer has been investigated by planar laser induced fluorescence as well as large eddy simulation (LES). In the case of swirling addition into the jet flow, there exists an optimized swirling jet angle or optimized jet-to-cross velocity ratio for the fixed mixer configuration. A larger swirling jet angle will make the flow dominated by the swirling, resulting in a slower mixing process. Interaction of swirling crossflow with no-swirling injected streams, or with swirling injected streams in the opposite direction is beneficial for the mixing. LES predictions show that many small vortices are produced homogenously due to intensified impingement in the case of opposite swirling directions, leading to a relative fast mixing process in several milliseconds. Whereas the mixing is restrained when the swirling directions of two flows are the same.

Key words: swirling, transverse jet mixer, process intensification, laser induced fluorescence, large eddy simulation

Introduction

Mixing is one of the most common used unit operations in industrial processes, especially in those with rapid parallel competitive reaction, nanoparticle precipitation or reactive polymerization, where the time scale of the reaction is milliseconds, thus requiring very fast mixing of the reactants. To achieve this, many researchers have devoted to optimize the mixer design. Mixers capable of rapid mixing include coaxial jet mixer [1,2], impinging jet mixer [3-5], transverse jet mixer with or without crossflow, and microchannel mixer [6-9]. The mixing time scale of these mixers can reach several to several tens of milliseconds. Despite all this, many researchers are exploring new ways to intensify the mixing process, e.g. adding swirling [10,11] or employing ultrasonication [12] in the flow field.

Swirling flows are widely used in the practical applications such as separation, mixing and flame stabilization [13], to intensify the mass, momentum and heat transfer process. Takano et al. [14] found that the maximum mass transfer coefficient by adding swirling flow can reaches 6 times larger than that of the straight pipe without swirling. Palsson et al. [15] found adding swirling flow into the heat exchanger pipes can increase the shear stress and reduce the fouling rate. Dong et al. [16] found that the rotation swirler is more efficient than the non-rotation swirler in reducing the pressure drop decrease and conveying energy in all ranges of the conveying velocity in dilute-phase pneumatic conveying. Musa et al. [17] studied the ignition and flame stability of high-density polyethylene solid fuel with incoming swirling air through a solid fuel ramjet

and found that inducing swirling flow can improve the combustion efficiency and stability. Liu et al. [18] studied the mixing performance in the turbulent swirling flow of a multi-inlet vortex reactor by using PLIF and the mixing mechanisms in the reactor were discussed. It is noted that reports on the swirling flow in the literatures mainly focus on gas mixing and few works can be found for the liquid mixing, which is more widely used in chemical production. Thus, it is essential to study how the swirling design affect the liquid mixing process in the traditional jet mixer.

The experimental techniques, e.g. particle image velocimetry (PIV) and laser-induced fluorescence (LIF) technique, as well as computational fluid dynamics (CFD), are commonly used to study the mixing process. The macroscale mixing characteristics such as the concentration distribution, jet penetration and trajectories can be obtained experimentally[19,20]. However, it is difficult to obtain the intrinsic features, e.g. the generation and evolution of the vortex structure. The CFD simulation provides an alternative method to study the mixing mechanisms in detail. For example, Zhang et al. [21] employed LES to investigate the variation of pressure and velocity of the oscillation caused by the unsteady engulfment flow. Huang et al. [22] investigated the effect of the density difference and viscosity of two miscible fluids on the mixing process in a lid-driven cavity by numerical simulation. Mohammadpour et al. [23] used CFD to understand the flow structure for the design of the packed bed. Kriaa et al. [24] studied the dynamic structure, heat and mass transfer of a vertical ceramic tiles dryer by using CFD. Zhang et al. [25] studied the mixing performance of a 3D metal printing showerhead mixer by both experiments and CFD simulation. In

these studies, CFD is employed to not only understand the flow structure but also optimize the mixer design.

The multi-orifice-impinging transverse (MOIT) jet mixer, in which the jet flow is injected into crossflow through multiple orifices, can accomplish fast liquid mixing in a few to tens of milliseconds in our previous study [26,27]. The objective of this work is to carry out further investigation on the mixing intensification when the swirling flow are added into the jet flow or the crossflow. The mixing process of different jet mixer configurations was firstly studied by using the PLIF technique. Then LES was employed to understand the interaction mechanisms between the jet flow and crossflow with and without adding swirling design.

Experimental

Mixer configurations and operation conditions

In this work, two configurations of swirling jet mixer are investigated. For the first configuration, as shown in Figure 1a, Stream A (or crossflow) directly flows through the mixing pipe. Stream B (or jet flow) is injected into the mixing pipe from four identical orifices which are embedded on the pipe wall. The swirling of the jet flows is generated by designing a swirling jet angle, θ_1, between the centerline of the jet orifice and the radial direction. For the other configuration, as shown in Figure 1b, the swirling is added not only into the jet flow, but also into the crossflow. The swirling crossflow is generated by injecting Stream A into the mixing pipe through four identical orifices embedded on the pipe wall with a swirling jet angle, θ_2,

between the centerline of the jet orifice and the radial direction. The rectangular chamber is constructed around the pipe to reduce the optical distortion caused by the round pipe. In order to distinguish the swirling direction of the jet flows, we define the swirling jet angle (θ_1 or θ_2) positive if the swirling is counterclockwise from the top view, otherwise, the swirling jet angle is negative when the swirling is clockwise. The swirling jet mixer shown in Figure 1 is named as M(θ_1, θ_2). In this study, the diameter of mixing pipe is fixed to be 16 mm, while the diameter of injecting orifice is fixed to be 4 mm, and the number of orifices, n, is 4. Different jet mixer configurations and operation conditions are listed in Table 1. The Reynolds numbers of the Stream A in the mixing pipe and the Stream B in the orifices, Re_A and Re_B, are in the range of 7000 - 17,500 and 3500 - 14,000, respectively, to ensure the two streams are in the turbulent flow. The Reynolds number of the completely mixed stream of two fluids, Re_M, is fixed to be 21000. As two fluids have the same density, the velocity ratio of the jet flow (Stream B) to the crossflow (Stream A) is defined to characterize the operation conditions,

$$r = u_j / u_c \tag{1}$$

where u_j is the velocity in the injecting orifice, u_c is the velocity of the crossflow in the mixing pipe.

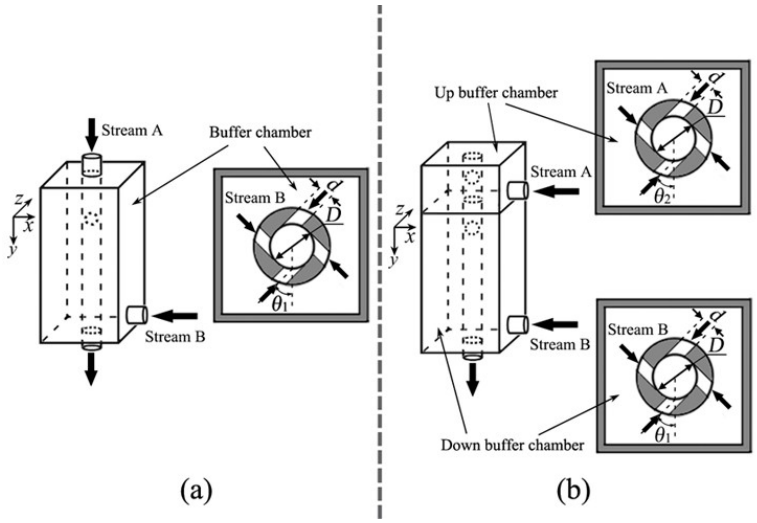

Figure 1. Schematic diagrams of the MOIT jet mixer with (a) adding swirling in the jet flow and (b) adding swirling in both the jet flow and the crossflow.

Table 1 Operating conditions for different configurations of the mixer investigated by PLIF and LES.

Case	Flow rate		*Re*			*r*	θ_1	θ_2
	Q_A (L/h)	Q_B (L/h)	$Re_A\times10^4$	$Re_B\times10^4$	$Re_M\times10^4$	u_B/u_A	°	°
1	800	160	1.75	0.35	2.1	0.8	0	0
2	640	320	1.40	0.70	2.1	2	0	0
3	480	480	1.05	1.05	2.1	4	0	0
4	384	576	0.84	1.26	2.1	6	0	0
5	320	640	0.70	1.40	2.1	8	0	0
6	800	160	1.75	0.35	2.1	0.8	15	0
7	640	320	1.40	0.70	2.1	2	15	0
8	480	480	1.05	1.05	2.1	4	15	0
9	384	576	0.84	1.26	2.1	6	15	0
10	320	640	0.70	1.40	2.1	8	15	0
11	800	160	1.75	0.35	2.1	0.8	30	0
12	640	320	1.40	0.70	2.1	2	30	0

13	480	480	1.05	1.05	2.1	4	30	0
14	384	576	0.84	1.26	2.1	6	30	0
15	320	640	0.70	1.40	2.1	8	30	0
16	800	160	1.75	0.35	2.1	0.8	45	0
17	640	320	1.40	0.70	2.1	2	45	0
18	480	480	1.05	1.05	2.1	4	45	0
19	384	576	0.84	1.26	2.1	6	45	0
20	320	640	0.70	1.40	2.1	8	45	0
21	480	480	1.05	1.05	2.1	4	0	45
22	384	576	0.84	1.26	2.1	6	0	45
23	320	640	0.70	1.40	2.1	8	0	45
24	480	480	1.05	1.05	2.1	4	30	45
25	480	480	1.05	1.05	2.1	4	15	45
26	480	480	1.05	1.05	2.1	4	-15	45
27	480	480	1.05	1.05	2.1	4	-30	45

Experimental setup

The experimental setup is shown in Figure 2. 2D LIF technique is employed to study the mixing performance of the swirling jet mixer. Tap water is used for both Stream A and Stream B, and Stream A dissolves a tracer for the PLIF experiment. Rhodamine 6G is chosen as the fluorescence tracer because of its relatively low sensitivity to temperature variations [28]. Both streams are pumped into the jet mixer at a fixed flow rate using two gear pumps. The entire fluid in the pipe is excited by a continuous laser (KSPL05), and the emitted fluorescence light is captured by a CCD camera (Baumer, TXG14NIR) with the image size of 1392 × 1040 pixels. The distribution of the fluorescence intensity in the measurement plane can be converted

to the tracer concentration distribution. The details of the experimental system and imaging post-processing can be found in our previous work [27].

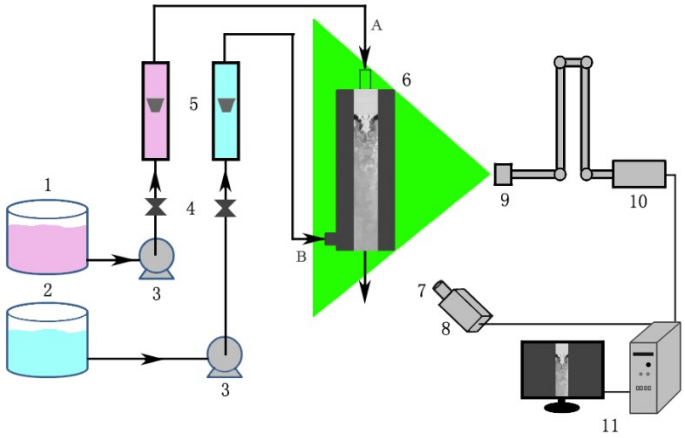

Figure 2. Experimental setup of the PLIF measuring device. 1-Rhodamine 6G tank; 2-Tap water tank; 3-Gear pump; 4-Flow valves; 5-Rotameter; 6-swirling jet mixer; 7-High-pass optical filter; 8-CCD camera; 9-Laser sheet; 10-KSPL05 laser; 11-Data acquisition and image processing system.

Numerical methods

Large eddy simulation (LES) approach is used to simulate the transient turbulence flow, in which large-scale eddies are predicted directly by solving Navier-Stokes equations, whereas small eddies are simulated by subgird scale models. The basic governing equations are as flows:

$$\frac{\partial \bar{u}_i}{\partial x_i}=0 \tag{2}$$

$$\frac{\partial \bar{u}_i}{\partial t}+\frac{\partial \bar{u}_i\bar{u}_j}{\partial x_j}=\frac{-1}{\rho}\frac{\partial \bar{p}}{\partial x_i}+\nu\frac{\partial^2 \bar{u}_i}{\partial x_i x_j}-\frac{\partial \tau_{ij}}{\partial x_i} \tag{3}$$

where u_i is the velocity component in i direction, ρ is the density, p is the pressure, ν is the kinematic viscosity and τ_{ij} is the SGS stress tensor, which represents the effect of the unresolved scales in the resolved ones and is written as

$$\tau_{ij}=\overline{u_i u_j}-\overline{u}_i\overline{u}_j \tag{4}$$

In order to close the equation, additional stress is expressed in terms of the grid-scale velocity field as

$$\tau_{ij}-\frac{1}{3}\delta_{ij}\tau_{kk}=-2\nu_t\overline{S}_{ij} \tag{5}$$

where S_{ij} is the filtered strain tensor in the eddy viscosity model. The dynamic kinetic energy (DKE) model, which is first proposed by Kim and Menon [29], is employed as SGS turbulent model. The DKE model calculates the subgrid kinetic energy by solving its transport equation, which has been successfully applied to simulate similar turbulent mixing processes [30]. The SGS kinetic energy, k_{sgs}, and SGS eddy viscosity, ν_t, are defined as

$$k_{sgs}=\frac{1}{2}\left(\overline{u_k^2}-\overline{u}_k^2\right) \tag{6}$$

$$\nu_t=C_k k_{sgs}^{1/2}\Delta_f \tag{7}$$

where Δ_f is the filter size defined as $V^{1/3}$. The SGS stress tensor, τ_{ij}, can be expressed as

$$\tau_{ij}-\frac{2}{3}k_{sgs}\delta_{ij}=-2C_k k_{sgs}^{1/2}\Delta_f\overline{S}_{ij} \tag{8}$$

Then, the transport equation for the SGS kinetic energy is

$$\frac{\partial \bar{k}_{sgs}}{\partial t}+\frac{\partial \bar{u}_j \bar{k}_{sgs}}{\partial x_j}=-\tau_{ij}\frac{\partial \bar{u}_i}{\partial x_j}-C_\varepsilon \frac{k_{sgs}^{3/2}}{\Delta_f}+\frac{\partial}{\partial x_j}\left(\frac{\nu_t}{\sigma_k}\frac{\partial k_{sgs}}{\partial x_j}\right) \tag{9}$$

where C_k and C_ε, are determined dynamically by solving the transport of the subgrid scale turbulence kinetic energy, and σ_k equals 1.0.

The transport equation for the passive scalar, f, is written as

$$\frac{\partial \bar{f}}{\partial t}+\bar{u}_i\frac{\partial \bar{f}}{\partial x_i}=\Gamma\frac{\partial}{\partial x_i}\left(\frac{\partial \bar{f}}{\partial x_i}\right)-\frac{\partial J_{i,sgs}}{\partial x_i} \tag{10}$$

where Γ is the molecular diffusivity and $J_{i,sgs}$ is the subgrid scalar flux vector, which can be modeled by using the gradient diffusion hypothesis as

$$J_{i,sgs}=\frac{-\nu_{sgs}}{Sc_{sgs}}\frac{\partial \bar{f}}{\partial x_i} \tag{11}$$

where ν_{sgs} is the viscosity or eddy viscosity and Sc_{sgs} is the turbulent Schmidt number.

The governing equations are solved by the commercial software ANSYS FLUENT 14.5.7. The SIMPLE algorithm is adopted for pressure-velocity coupling, and the bounded central differencing method is used for the spatial discretization of the momentum, turbulent kinetic energy, and concentration. Time step is set to 0.0002 s. The mesh generation method, boundary condition setting and grid sensitivity analysis has been discussed in our previous work [26] and is also adopted in this work.

Results and discussion

Macromixing performance by adding swirling flow

To evaluate the effect of the swirling design on the macromixing performance, PLIF experimental results for different mixer configurations are firstly discussed. Here, the strategy of adding swirling flow into injected streams (Stream B) is first considered. The Reynolds number, $Re_{M,}$ of the mixed stream is kept at 21000 when the jet-to-cross velocity ratio, r, is varied from 0.8 to 8.

The swirling of the jet flow are generated when θ_1 increases from 0° (without swirling design) to 15°, 30°, and 45°. Instantaneous concentration distributions at different jet-to-cross velocity ratio are shown in Figure 3. It is observed for a certain configuration of the jet mixer, increasing r leads to high interaction intensity between injected streams and the crossflow. When r reaches a certain value, strong impingement results in the occurrence of the back-splash, i.e. part of injected streams go upstream. One can see that there exist two types of the back-splash behavior. One is that the back-splash stream goes upstream in the middle of the mixing pipe, as shown in Figures $3d_1$ and $3e_1$, i.e. the configuration without swirling flow design. The other is that the back-splash stream goes upstream adjacently to the mixing pipe wall when the swirling flow is added into the jet flow, as shown in Figures $3d_3$, $3e_3$, $3c_4$, $3d_4$, $3e_4$.

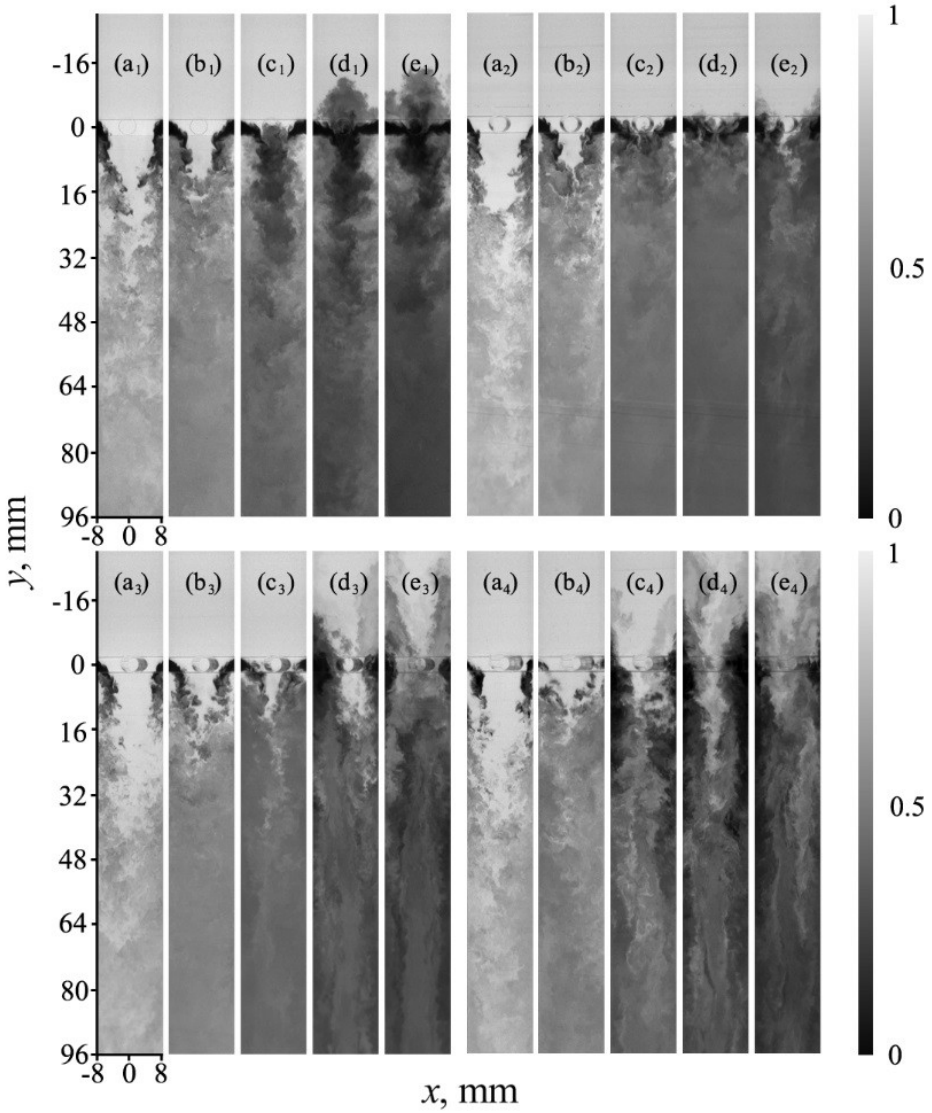

Figure 3. Instantaneous concentration distributions for different mixer configurations. (a_1-e_1): M(0°, 0°), (a_2-e_2): M(15°, 0°), (a_3-e_3): M(30°, 0°), (a_4-e_4): M(45°, 0°); (a_1-a_4): r = 0.8, (b_1-b_4): r = 2, (c_1-c_4): r = 4, (d_1-d_4): r = 6, (e_1-e_4): r = 8.

In addition, one can see that slight back-splash occurs when r = 8 for the configuration of M(15°, 0°), whereas intensive back-splash has occurred when r reaches 6 for the mixer without swirling addition (as shown in Figure 3d_1), i.e. the back-splash can be effectively suppressed with a larger jet-to-cross velocity ratio by adding swirling into the jet flow. It is noted that the overall mixing time increases

when the back-splash occurs, which indeed represents axial back-mixing. In the cases of swirling addition, obvious back-splash is also observed when r = 6 for M(30°, 0°) and r = 4 for M(45°, 0°). This indicates that there is an optimized swirling jet angle for generating swirling flow with appropriate intensity.

In order to evaluate the macromixing performance quantitatively, the mixing time is calculated based on the intensity of segregation (*IOS*) of the mixed stream in the pipe at a certain axial location. The *IOS* is defined by

$$IOS^{0.5} = \frac{\sigma_t}{\sqrt{\langle \bar{f}_t \rangle \left(1 - \langle \bar{f}_t \rangle\right)}} \tag{12}$$

where $\langle \bar{f}_t \rangle$ is the mean concentration, σ_t is the deviation. The overall mixing time τ is defined as

$$\tau = \frac{L}{u_M} \tag{13}$$

where L is the distance from the upstream point where $IOS^{0.5} = 0.1$ to the downstream point where the two streams have reached the same mixing state, $IOS^{0.5} = 0.1$.[31]

As shown in Figure 4, for a certain jet mixer, there is an optimum velocity ratio to obtain the shortest mixing time, e.g. r = 6 is the optimum velocity ratio for the mixer M(15°, 0°), with an overall mixing time of τ = 3.8 ms. At the same time, for a certain velocity ratio, there is also an optimized swirling jet angle design. M (15°, 0°) is the optimized mixer when velocity ratios are 4, 6 and 8, while M (30°, 0°) is the

optimum mixer when velocity ratio are 0.8 and 2, respectively, which indicates that lower jet-to-cross velocity ratio requires a larger swirling jet angle to guarantee appropriate impingement intensity of two flows.

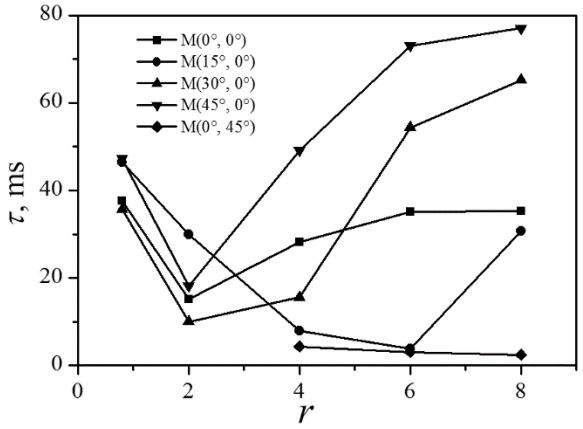

Figure 4. Comparison of the overall mixing time for different mixer configurations.

However, when the swirling flow is added into the crossflow (Stream A) the macromixing performance shows significant difference. For the convenience of comparison, the mixing performance of M(0°, 45°) and M(0°, 0°) at the velocity ratios of r = 4, 6, 8 are compared, as shown in Figure 5. It is seen that the concentration distribution in the mixer M(0°,45°) becomes homogeneous much earlier. Besides, the back-splash does not occur even at r = 8, i.e. the back-splash can be effectively suppressed by adding swirling flow into the crossflow. From Figure 4, we can find that the mixing times of M(0°,45°) are 4.3 ms, 3.0 ms and 2.4 ms at the velocity ratios of r = 4, 6, 8, which is much shorter than that of M(0°, 0°) (i.e. without swirling addition). It can be concluded that adding swirling flow into the crossflow can greatly speeds up the mixing process.

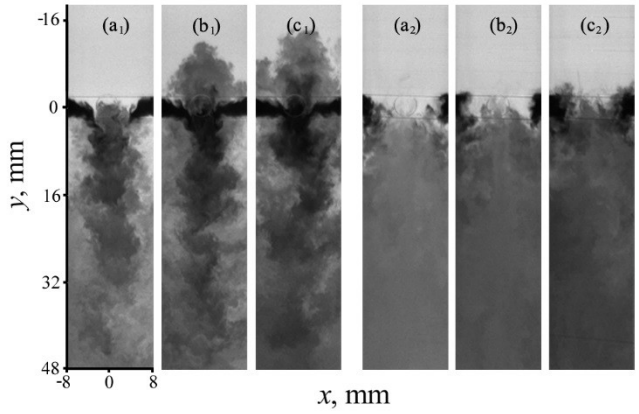

Figure 5. The instantaneous concentration distribution of different jet mixer. (a_1, b_1, c_1): M(0°, 0°), (a_2, b_2, c_2): M(0°,45°); (a_1, a_2): $r = 4$, (b_1, b_2): $r = 6$, (c_1, c_2): $r = 8$.

Validation of LES predictions

In order to understand the interaction mechanisms of the mixing fluids using different swirling adding strategies, the LES simulations are carried out. Firstly, prediction accuracy is performed. As the grid sensitivity analysis has been carried out in our previous work [26], here we only validate the simulation results from the wall y^+ value discussion, power spectral density analysis and time-averaged concentration distribution comparison.

The y^+ value is the dimensionless wall distance, which should be smaller than 5 to ensure that the flow adjacent to the wall is in the laminar regime. In the study, for all the simulation cases, at least 95% of cells in the near-wall region of the mixing pipe has $y^{+¿¿}$ values below the critical value, 5, which indicates that the viscous sublayer can be resolved well in the mixing zone.

The power spectral density (PSD) is usually used to understand the transport of coherent structures and the related energy dissipation process. In the LES modeling,

the criteria for a grid of sufficient fineness is that it can resolve the inertial range to get meaningful results[32]. According to the Kolmogorov -5/3 theory, the characteristic slop (-5/3) of the inertial range can be used for the test. The concentration PSD of M(0°, 0°), M(15°, 0°), M(30°, 0°), M(45°, 0°) and M(0°, 45°) at three selected points, i.e. $x = 0$, $y/D = 3, 4, 5$ are analyzed. The Kolmogorov's -5/3 decay is supported in the intermediate frequencies of 50-500 Hz. It can be assumed that the grid resolution is sufficient for the simulation.

Figure 6 compares the time-averaged concentration distribution between PLIF experiments and LES predictions. As can be seen, the predicted concentration distributions of all swirling jet mixers agree well with the experimental results. The above analysis shows that the LES method adopted in this study can well predict the turbulent mixing process

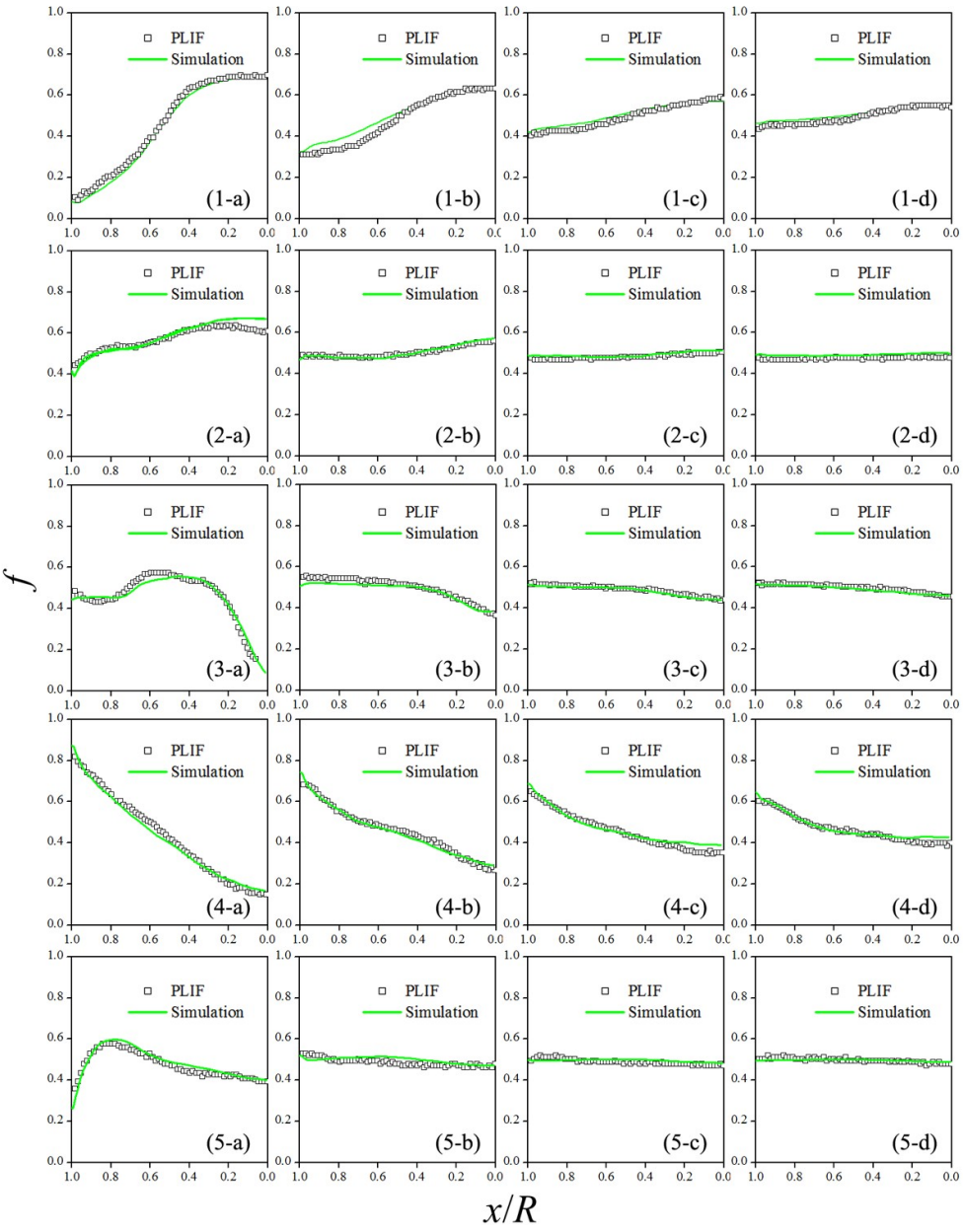

Figure 6. Comparison of the time-averaged concentration distributions between the PLIF results and the LES predictions. (1) M(0°,0°); (2) M(15°,0°); (3) M(30°,0°); (4) M(45°,0°); (5) M(0°,45°); r =4, 0< x/R < 1; (1a~5a): y/D = 0.5; (1b~5b): y/D = 1.0; (1c~5c): y/D = 1.5; (1d~5d): y/D = 2.0.

Understanding swirling effect by velocity distribution analysis

In the jet mixing process, how injected streams interact with the bulk flow

determines the mixing efficiency. Thus, predicted velocity distribution is illustrated to understand the interaction mechanisms when swirling is employed. Figure 7 shows the mean *x*-velocity contours and streamlines in the case of swirling addition into injected streams at $r = 4$. It is seen that symmetrical backflow vortexes occur near the pipe wall due to the entrainment of injected streams when no swirling is added (Figure 7a). When a swirling jet angle of 15° is applied in the jet flow, injected streams are found distorted and smaller vortexes are generated, as shown in Figure 7b. In addition, streamlines become more complicated, which implies that impingement of two fluids has been intensified by the swirling addition. However, when the swirling jet angle increases to 30°, backflow vortexes disappear and an irregular whirlpool occurs. This indicates that the enhanced swirling flow surpasses the interaction between the jet and the crossflow. One can see that a more regular whirlpool is generated when the swirling jet angle further increases to 45° (see Figure 7d). It is noted that when the swirling dominates the fluid flow, injected streams will rotate down adjacently to the wall of the mixing pipe, whereas the crossflow prefer to flow down in the center of the pipe. This flow of relative segregation is actually not conducive to mixing. Comparison of the overall mixing time in Figure 4 gives a direct support of this point, i.e. the order of mixing time for different jet mixers is M(15°, 0°) < M(30°, 0°) < M(0°, 0°) < M(45°, 0°) when $r = 4$. Thus, appropriate swirling jet angle should be 15° when the swirling is applied in the jet flow.

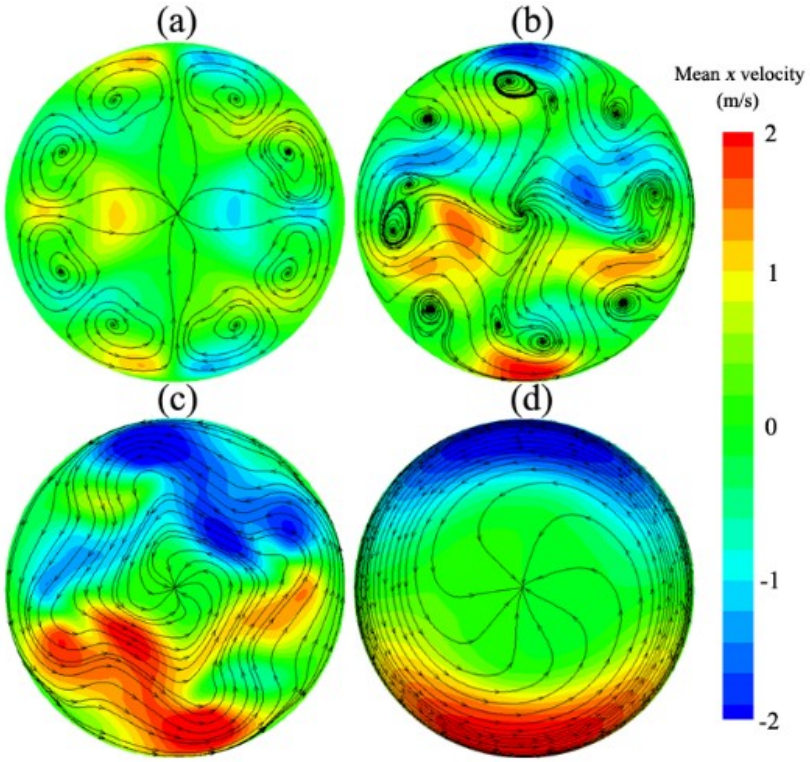

Figure 7. The contours of the mean x-velocity and the streamlines at $y/D = 0.25$.

(a) M(0°, 0°); (b) M(15°, 0°); (c) M(30°, 0°); (d) M(45°, 0°)

In the case of adding swirling in both the jet flow and the crossflow, the mixing process is significantly different when the swirling directions of two streams are changed. Here, the swirling jet angle of the crossflow, θ_2 is fixed at 45°, and the swirling jet angle of injected streams, θ_1 is varied from opposite direction (i.e. θ_1 = -30° or -15°), no swirling (i.e. θ_1 = 0°), to the same direction (i.e. θ_1 =15 or 30°). Figure 8 compares the velocity distribution colored by the mean tangential velocity. It is seen that the swirling is speed up when the swirling directions are the same (Figures 8a and 8b). Whereas the tangential velocities decrease significantly when the swirling directions are opposite (see Figures 8d and 8e). This implies that the energy of two swirling streams is effectively dissipated due to the strong impingement between the

crossflow and injected streams, which is indeed beneficial for improving the mixing efficiency. The profile of the overall mixing time *vs.* the swirling jet angle of θ_1 (Figure 9) gives a direct proof of this point. It is seen that the mixing time decreases obviously from 31.4 ms to 6.1~7.2 ms when θ_1 changes from a same direction (30°) to 0° or an opposite direction (-15° and -30°). In addition, there is no significant difference in the mixing time when the swirling directions are opposite or injected streams have no swirling.

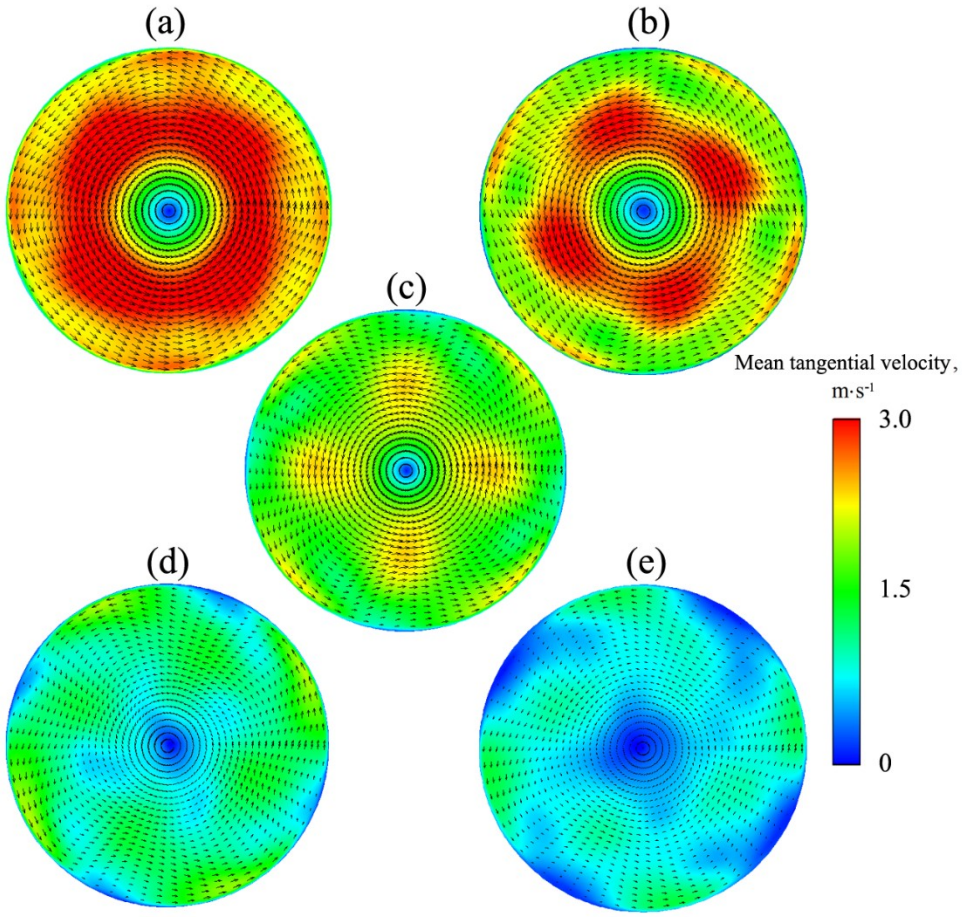

Figure 8. Velocity distribution on the cross plane at y/D = 0.5 colored by the mean tangential velocity. (a) M(30°,45°); (b) M(15°,45°); (c) M(0°,45°); (d) M(-15°,45°); (e) M(-30°,45°).

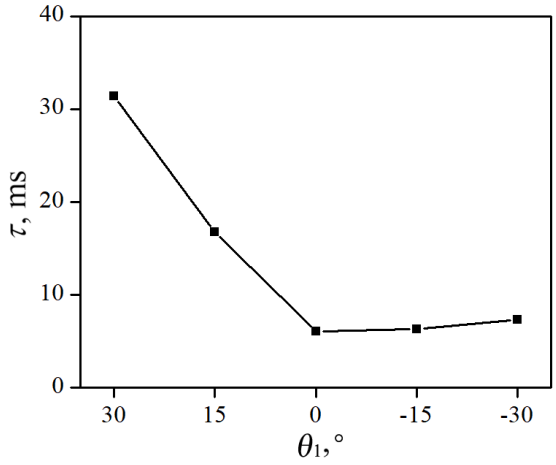

Figure 9. The overall mixing time of the jet mixer with different swirling angles of injected streams, $r = 4$, $\theta_2 = 45°$.

Vorticity evaluation

In order to deeply analyze the swirling effect on the mixing process, the formation and development of the vortex structures are evaluated by the Q-criterion, which is one of the most popular criteria to visualize the flow structure by identifying the invariants of the velocity gradient tensor.

Figure 10 shows the vortices number increases obviously when the swirling jet angle of injected streams increase from 0° to 15° in the case of $\theta_2 = 0°$. This implies the turbulent interaction is intensified, leading to a fast mixing process, as shown in Figure 4. However, further increase in the swirling jet angle to 30° and 45°, the vortices number begin to decrease. Especially for the jet mixer M(45°, 0°), there are fewer vortices downstream but many vortices appear upstream, resulting in obvious back mixing and the overall mixing time is extended.

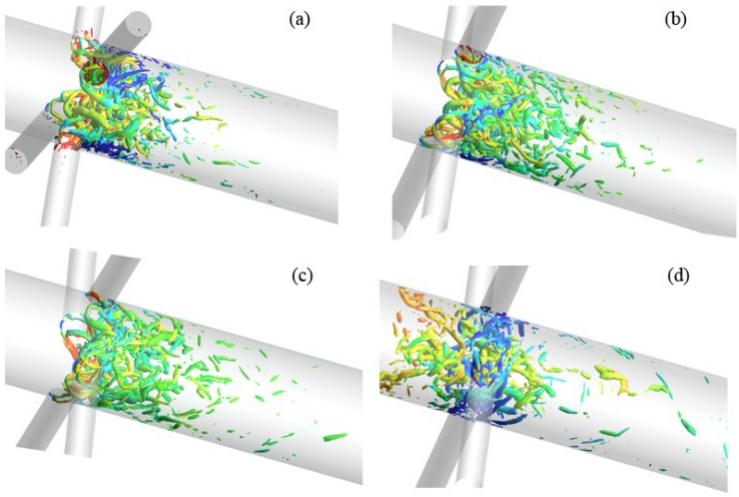

Figure 10. Visualization of the turbulent vortex structure by three-dimensional iso-contours of Q-criterion ($Q = 5\times10^6$), colored by the concentration distribution. (a) M(0°, 0°); (b) M(15°, 0°); (c) M(30°, 0°); (d) M(45°, 0°).

Figure 11 provides a qualitative comparison of the turbulent structures identified using the isonormalized Q-criterion at the cross sections of y/D =0.5. Here, θ_2 is fixed at 45° and the swirling jet angle of injected streams, θ_1 varies from 30° to -30°. It is seen that the vortex distribution is more homogeneous with smaller vortices in the cases of no swirling addition into the jet flow or opposite swirling directions between the jet flow and the crossflow. In particular, for the mixer of M(30°,45°) and M(15°,45°), large vortices accumulate in the center of the mixing pipe, indicating that the same swirling directions between two flows will speed up the rotation of the mixed stream. Correspondingly, the interaction intensity becomes weak, thus, leading to longer mixing time.

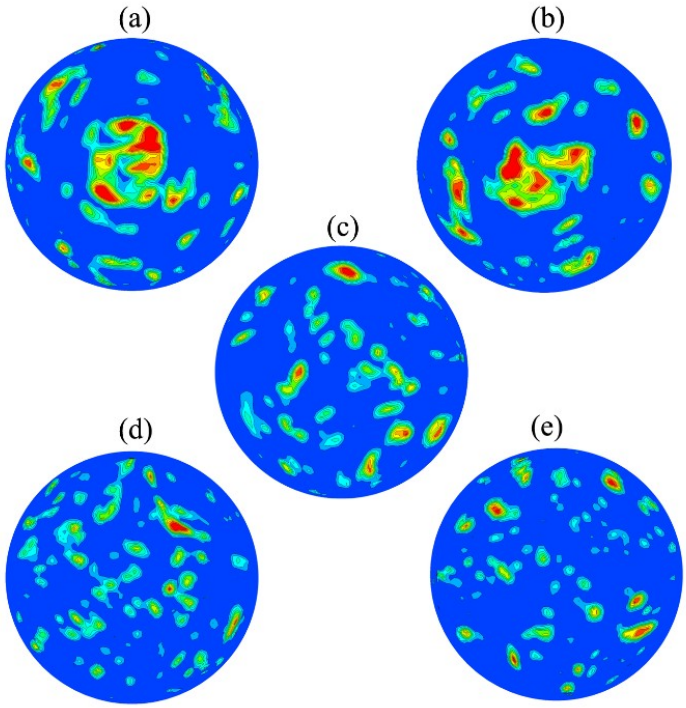

Figure 11. Turbulent structures from the LES identified using the isonormalized Q-criterion, $y/D = 0.5$. (a) M(30°, 45°); (b) M(15°, 45°); (c) M(0°, 45°); (d) M(-15°, 45°); (e) M(-30°, 45°).

Conclusions

In this work, the effect of swirling addition on the mixing performance of multi-orifice-impinging transverse jet mixer has been studied experimentally and numerically. The swirling is added into injected streams, the crossflow, or the both through eccentric jet orifices. The mixing performance of different mixer configurations is evaluated by the overall mixing time, concentration and velocity distribution, and vorticity analysis.

When swirling is only added into the jet flow, the back-splash can be suppressed at a relative larger jet-to-cross velocity ratio (r) compared with the traditional multi-

orifice-impinging transverse jet mixer. There exists an optimum operating velocity ratio for a fixed configuration, or an optimum design of the swirling jet angle for a fixed velocity ratio. LES predictions show that the mixing process is intensified by producing more small vortices with an appropriate swirling jet angle. Whereas a larger swirling jet angle will make the flow dominated by the swirling other than intensification of the interaction between two flows.

In the case of adding swirling into only crossflow or into both flows, interaction of swirling crossflow with no-swirling injected streams, or with swirling injected streams in the opposite direction is beneficial for the mixing intensification. Many small vortices are produced due to intensified interaction, resulting in a relative fast mixing process in several milliseconds. However, when the swirling directions of two flows are the same, large vortices accumulate in the center of the mixing pipe, resulting in weak interaction between two flows and relative slower mixing process.

Acknowledgements

We acknowledge the financial support from the National Natural Science Foundation of China (Grant No. 21476048, 22078058), Preliminary Research Project Fund of General Equipment Department, and the Postgraduate Research & Practice Innovation Program of Jiangsu Province (Grant No. KYCX18_0131).

References

1. Zhou MM, Bai DH, Zong Y, et al. Numerical investigation of turbulent reactive mixing in a novel coaxial jet static mixer. *Chem Eng Process.* 2017;122:190-203.

2. Hassel E, Jahnke S, Kornev N, et al. Large-eddy simulation and laser diagnostic measurements of mixing in a coaxial jet mixer. *Chem Eng Sci.* 2006;61(9):2908-2912.

3. Liu WJ, Ma CY, Liu JJ, et al. Continuous reactive crystallization of pharmaceuticals using impinging jet mixers. *AlChE J.* 2017;63(3):967-974.

4. Metzger L, Kind M. On the mixing in confined impinging jet mixers - Time scale analysis and scale-up using CFD coarse-graining methods. *Chem Eng Res Des.* 2016;109:464-476.

5. Fonte CP, Sultan MA, Santos RJ, et al. Flow imbalance and Reynolds number impact on mixing in Confined Impinging Jets. *Chem Eng J.* 2015;260:316-330.

6. Liu MY. Computational study of convective-diffusive mixing in a microchannel mixer. *Chem Eng Sci.* 2011;66(10):2211-2223.

7. Duryodhan VS, Chatterjee R, Singh SG, et al. Mixing in planar spiral microchannel. *Exp Therm Fluid Sci.* 2017;89:119-127.

8. Chen SY, Zhang T, Lv L, et al. Intensification of the liquid side mass transfer in double-side falling film microchannels by micro-mixing structures. *Chem Eng Sci.* 2019;193:264-275.

9. Song Y, Shang MJ, Li GX, et al. Influence of mixing performance on polymerization of acrylamide in capillary microreactors. *AlChE J.* 2018;64(5):1828-1840.

10. Fang N, Zeng L, Zhang B, et al. Numerical simulation of flow and gasification characteristics with different swirl vane angles in a 2000 t/d GSP gasifier. *Appl Therm Eng.* 2019;153:791-799.

11. Zhang F, Wang X, Li J. Numerical investigation of flow and heat transfer characteristics in radial pre-swirl system with different pre-swirl nozzle angles. *Int J Heat Mass Transfer.* 2016;95:984-995.

12. Maitra A, Bagchi S. Study of solute–solvent and solvent–solvent interactions in pure and mixed binary solvents. *J Mol Liq.* 2008;137(1-3):131-137.

13. Kharoua N, Khezzar L, Alshehhi M. The interaction of confined swirling flow with a conical bluff body: Numerical simulation. *Chem Eng Res Des.* 2018;136:207-218.

14. Takano T, Ikarashi Y, Uchiyama K, et al. Influence of swirling flow on mass and momentum transfer downstream of a pipe with elbow and orifice. *Int J Heat Mass Transfer.* 2016;92:394-402.

15. Palsson H, Beaubert F, Lalot S. Inducing Swirling Flow in Heat Exchanger

Pipes for Reduced Fouling Rate. *Heat Transfer Eng.* 2013;34(8-9):761-768.
16. Dong L, Rinoshika A. Comparison between rotation swirler and non-rotation swirler in a horizontal swirling flow pneumatic conveying. *Powder Technol.* 2019;346:396-402.
17. Musa O, Chen X, Zhou CS. Experimental and numerical investigation on the ignition and combustion stability in solid fuel ramjet with swirling flow. *Acta Astronaut.* 2017;137:157-167.
18. Liu ZP, Hitimana E, Olsen MG, et al. Turbulent mixing in the confined swirling flow of a multi-inlet vortex reactor. *AlChE J.* 2017;63(6):2409-2419.
19. Kartaev EV, Emel'kin VA, Ktalkherman MG, et al. Analysis of mixing of impinging radial jets with crossflow in the regime of counter flow jet formation. *Chem Eng Sci.* 2014;119:1-9.
20. Kartaev EV, Emelkin VA, Ktalkherman MG, et al. Formation of counter flow jet resulting from impingement of multiple jets radially injected in a crossflow. *Exp Therm Fluid Sci.* 2015;68:310-321.
21. Zhang J-w, Liu S-f, Cheng C, et al. Investigation of three-dimensional flow regime and mixing characteristic in T-jet reactor. *Chem Eng J.* 2019;358:1561-1573.
22. Huang FL, Wang DF, Li ZP, et al. Mixing process of two miscible fluids in a lid-driven cavity. *Chem Eng J.* 2019;362:229-242.
23. Mohammadpour K, Alkhalaf A, Specht E. CFD simulation of cross-flow mixing in a packed bed using porous media model and experimental validation. *Comput Part Mech.* 2019;6(2):157-162.
24. Kriaa W, Bejaoui S, Mhiri H, et al. Study of dynamic structure and heat and mass transfer of a vertical ceramic tiles dryer using CFD simulations. *Heat Mass Transfer.* 2014;50(2):235-251.
25. Zhang HM, Kopfmuller T, Achermann R, et al. Accessing multidimensional mixing via 3D printing and showerhead micromixer design. *AlChE J.* 2020;66(4).
26. Luo PC, Fang Y, Wu B, et al. Turbulent characteristics and design of transverse jet mixers with multiple orifices. *Ind Eng Chem Res.* 2016;55(32):8858-8868.
27. Luo P, Jia H, Xin C, et al. An experimental study of liquid mixing in a multi-orifice-impinging transverse jet mixer using PLIF. *Chem Eng J.* 2013;228:554-564.
28. Crimaldi JP. Planar laser induced fluorescence in aqueous flows. *Exp Fluids.* 2008;44(6):851-863.
29. Kim W-W, Menon S. Application of the localized dynamic subgrid-scale model to turbulent wall-bounded flows. *AIAA, 35th Aerospace Sciences Meeting & Exhibit*. Reno, NV1997.
30. Nguyen TD, Harmand S. Heat transfer and vortical structures around a rotating cylinder with a spanwise disk and low-velocity crossflow. *Int J Heat Mass Transfer.* 2013;64:1014-1030.
31. Luo P, Tai Y, Fang Y, et al. Mixing times in single and multi-orifice-

impinging transverse (MOIT) jet mixers with crossflow. *Chin J Chem Eng.* 2016;24(7):825-831.

32. Sarikurt FS, Hassan YA. Large eddy simulations of erosion of a stratified layer by a buoyant jet. *Int J Heat Mass Transfer.* 2017;112:354-365.